SALSA: A Sequential Alternating Least Squares Approximation Method for MIMO Channel Estimation

Sepideh Gherekhloo, Khaled Ardah, and Martin Haardt, *Fellow, IEEE*

***Abstract*—In this article, we consider the channel estimation problem in sub-6 GHz uplink wideband multiple-input multiple-output (MIMO)-orthogonal frequency-division multiplexing (OFDM) communication systems, where a user equipment with a fully-digital beamforming structure is communicating with a base station having a hybrid analog-digital (HAD) beamforming structure. A novel channel estimation method called Sequential Alternating Least Squares Approximation (SALSA) is proposed by exploiting a hidden tensor structure in the uplink measurement matrix. Specifically, by showing that any MIMO channel matrix can be approximately decomposed into a summation of R factor matrices having a Kronecker structure, the uplink measurement matrix can be reshaped into a 3-way tensor admitting a Tucker decomposition. Exploiting the tensor structure, the MIMO channel matrix is estimated sequentially using an alternating least squares (ALS) method. Detailed simulation results are provided showing the effectiveness of the proposed SALSA method as compared to the classical least squares and linear minimum mean squared-error (LMMSE) methods.**

***Index Terms*—Channel estimation, massive MIMO, tucker tensor decomposition, alternating least squares, linear minimum mean squared-error.**

I. Introduction

Massive multiple-input multiple-output (MIMO) [1] is one of the key enabling technologies of 5G-NR mobile communications [2] and it shall remain relevant in future 6G wireless systems. By employing a large number of antennas at the base station (BS) relative to the number of scheduled users, massive MIMO systems increase the data throughput relative to legacy systems by providing a large beamforming gain and an improved multi-user interference suppression owing to its high spatial resolution [3]. Recently, massive MIMO communications have received a special attention with the introduction of millimeter-wave (mm-wave)-based wireless communications [4], since the use of massive MIMO in such systems becomes a requirement rather than an option to compensate the high pathloss encountered in the wireless communications at higher frequencies. However, it is well-known that the promised theoretical massive MIMO gains heavily rely on the availability of accurate channel state information (CSI) and the considered beamforming structure.

On the one hand, classical fully-digital (FD) beamforming structures, which generally provide the maximum beamforming gain, require a dedicated radio frequency (RF) chain for each antenna element. This increases not only the implementation cost and complexity of massive MIMO systems, but also the circuit energy consumption. A promising solution to these issues relies on the recently introduced hybrid analog-digital (HAD) beamforming structures [4], [5], [6], [7], [8], which use a combination of analog beamforming in the RF domain and digital beamforming in the baseband domain to reduce the number of RF chains as compared to FD beamforming structures, e.g., the number of RF chains can be as small as the number of transmitted data streams.

On the other hand, in 5G-NR systems, for example, the BS estimates the CSI from uplink sounding reference signals (SRS) emitted by the user terminals (UEs). In mm-wave systems, the CSI estimation problem is often transformed into a multi-dimensional direction-of-arrival (DoA) estimation problem [9], [10], [11], thanks to the low-rank (sparse) nature of mm-wave MIMO channels [4], where several techniques, e.g., compressed sensing [9], [10] and ESPRIT [11], [12] can be readily employed to obtain a high CSI estimation accuracy while requiring a small number of training overhead. Differently, in sub-6 GHz-based systems, the MIMO channels often experience a high-rank nature, which makes most, if not all, mm-wave-based MIMO channel estimation methods unfeasible. To this end, classical channel estimation techniques, e.g., least-squares (LS) and linear minimum mean squared-error (LMMSE) methods [13], [14] can be used to estimate sub-6 GHz-based MIMO channels. However, these methods were originally developed for single-antenna and small-scale MIMO systems. Moreover, the LS-based method suffers from a severe performance degradation in difficult scenarios, e.g., with a small number of training snapshots and/or a low signal-to-noise ratio (SNR). On the other hand, the LMMSE-based methods require some prior estimation of the statistical channel correlation matrix and noise variance, which makes it challenging to realize LMMSE in practice [15], [16]. Since sub-6 GHz massive MIMO communications are, and will remain, an integral part of current and future wireless communication systems, more efficient channel estimation techniques than the classical methods are required.

In this article, we consider the channel estimation problem in sub-6 GHz uplink wideband MIMO-OFDM communication systems, where a single-user with a FD beamforming structure communicates with a BS having a HAD beamforming structure. As the main contribution, we propose a novel channel estimation method called **S**equential **A**lternating **L**east **S**quares **A**pproximation (**SALSA**) by exploiting *a hidden tensor structure* in the uplink measurement matrix. Specifically, by showing that any MIMO channel matrix can be approximately decomposed into a summation of R factor matrices having a Kronecker structure. In this case, the uplink measurement matrix can be reshaped into a 3-way tensor admitting a Tucker decomposition [17]. Exploiting such a tensor representation, the MIMO channel matrix can be estimated sequentially using the classical alternating least squares (ALS) method [18]. Detailed simulation results are provided showing that the SALSA-based approach can achieve a more accurate channel estimation in difficult scenarios as compared to the classical LS- and LMMSE-based approaches.

Finally, we note that several tensor-based channel estimation methods have been proposed in the literature, e.g., [17], [18], [19], [20], [21], [22], [23], and references therein. However, these methods exploit simplified design assumptions on the antenna array structure and channel matrices, which generally lead to a relatively straightforward tensor modeling. Nonetheless, practical channel models, e.g., the 3GPP clustered delay line (CDL) channel model [24], [25], do not necessarily comply with these assumptions, and therefore, the existing methods, in many cases, cannot be employed. On the other hand, the

Manuscript received 3 April 2023; revised 20 November 2023; accepted 18 December 2023. Date of publication 26 December 2023; date of current version 16 May 2024. The review of this article was coordinated by Prof. Mugen Peng. *(Corresponding authors: Sepideh Gherekhloo; Martin Haardt.)*

Sepideh Gherekhloo and Martin Haardt are with the Communications Research Laboratory, Ilmenau University of Technology, 98693 Ilmenau, Germany (e-mail: sepideh.gherekhloo@tu-ilmenau.de; martin.haardt@tu-ilmenau.de).

Khaled Ardah is with Lenovo (Deutschland) GmbH, 70563 Stuttgart, Germany (e-mail: kardah@lenovo.com).

Digital Object Identifier 10.1109/TVT.2023.3347290

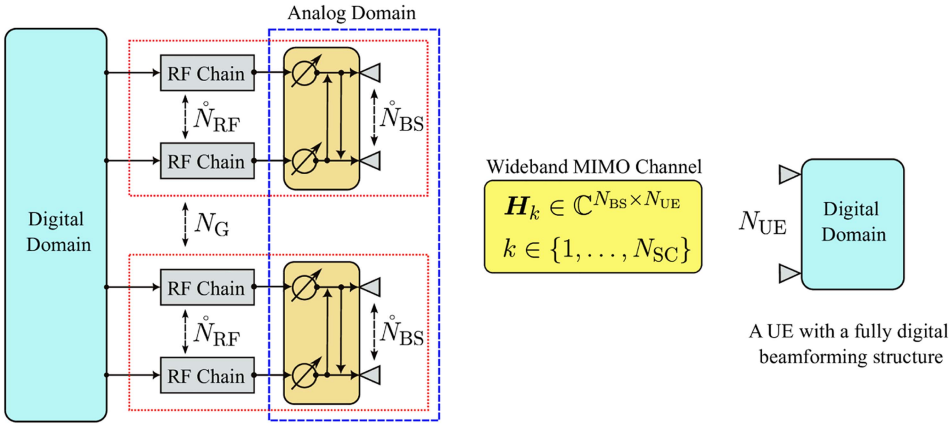

Fig. 1. Uplink MIMO-OFDM communication system.

proposed SALSA method does not require these assumptions on the channel model, which renders it very general and appealing for practical implementations.

Notation: The transpose, the complex conjugate, the conjugate transpose (Hermitian), and the Kronecker product are denoted as $\boldsymbol{A}^{\mathsf{T}}$, $\boldsymbol{A}^{*}$, $\boldsymbol{A}^{\mathsf{H}}$, and $\otimes$, respectively. Moreover, vec$\{\boldsymbol{A}\}$ forms a vector by staking the columns of $\boldsymbol{A}$ over each other, stack$\{\boldsymbol{A}_1, \ldots, \boldsymbol{A}_n\}$ forms a matrix by stacking $\boldsymbol{A}_1, \ldots, \boldsymbol{A}_n$ over each other, and blkdiag$\{\boldsymbol{A}_1, \ldots, \boldsymbol{A}_n\}$ forms a block-wise diagonal matrix by placing $\boldsymbol{A}_1, \ldots, \boldsymbol{A}_n$ on its main diagonal. The n-mode product of a tensor $\boldsymbol{\mathcal{A}} \in \mathbb{C}^{I_1 \times I_2 \times \ldots, \times I_N}$ with a matrix $\boldsymbol{B} \in \mathbb{C}^{J \times I_n}$ is denoted as $\boldsymbol{\mathcal{A}} \times_n \boldsymbol{B}$.

II. System Model

We consider an uplink single-user wideband MIMO-OFDM communication system, as depicted in Fig. 1, where a UE with N_{UE} antennas is communicating with a BS with N_{BS} antennas over N_{SC} subcarriers. The UE has a FD beamforming structure while the BS has a HAD beamforming structure with $N_{\mathrm{RF}} \leq N_{\mathrm{BS}}$ radio-frequency (RF) chains. We assume that the N_{BS} antennas and the N_{RF} RF chains are divided *equally*[1] into $N_{\mathrm{G}} \geq 1$ groups, where each group has $\mathring{N}_{\mathrm{BS}} = \frac{N_{\mathrm{BS}}}{N_{\mathrm{G}}}$ antennas and $\mathring{N}_{\mathrm{RF}} = \frac{N_{\mathrm{RF}}}{N_{\mathrm{G}}}$ RF chains (i.e., $N_{\mathrm{BS}} = N_{\mathrm{G}} \cdot \mathring{N}_{\mathrm{BS}}$ and $N_{\mathrm{RF}} = N_{\mathrm{G}} \cdot \mathring{N}_{\mathrm{RF}}$) and the RF chains in every group are connected with every antenna element in the same group.

We assume a block-fading channel model, where the channel coherence-time T_{C} is divided into $T_{\mathrm{BS}} T_{\mathrm{UE}}$ transmission time intervals (TTIs), i.e., every block has T_{UE} snapshots. The received signal by the BS in the (i,j)th TTI over the kth subcarrier, with $i \in \{1, \ldots, T_{\mathrm{BS}}\}$, $j \in \{1, \ldots, T_{\mathrm{UE}}\}$, $k \in \{1, \ldots, N_{\mathrm{SC}}\}$, can be expressed as

$$\bar{\boldsymbol{y}}_{k,i,j} = \bar{\boldsymbol{A}}_i^{\mathsf{H}} \boldsymbol{H}_k \boldsymbol{f}_{k,j} s_{k,j} + \bar{\boldsymbol{A}}_i^{\mathsf{H}} \bar{\boldsymbol{z}}_{k,i,j} \in \mathbb{C}^{N_{\mathrm{RF}}}, \tag{1}$$

where $\boldsymbol{f}_{k,j} \in \mathbb{C}^{N_{\mathrm{UE}}}$ is the (k,j)th precoding vector, $s_{k,j} \in \mathbb{C}$ is the training symbol, $\bar{\boldsymbol{z}}_{i,j} \in \mathbb{C}^{N_{\mathrm{BS}}}$ is the BS additive white Gaussian noise with zero mean and variance σ_n^2, and $\boldsymbol{H}_k \in \mathbb{C}^{N_{\mathrm{BS}} \times N_{\mathrm{UE}}}$ is the kth subcarrier frequency-domain MIMO channel matrix. Moreover, $\bar{\boldsymbol{A}}_i \in \mathbb{C}^{N_{\mathrm{BS}} \times N_{\mathrm{RF}}}$ denotes the analog combining matrix at the ith block at the BS, which has a block-diagonal structure given as[2]

$$\bar{\boldsymbol{A}}_i = \frac{1}{\sqrt{\mathring{N}_{\mathrm{BS}}}} \cdot \mathrm{blockdiag}\{\bar{\boldsymbol{A}}_{i,1}, \ldots, \bar{\boldsymbol{A}}_{i,N_{\mathrm{G}}}\} \in \mathbb{C}^{N_{\mathrm{BS}} \times N_{\mathrm{RF}}}, \tag{2}$$

where $\bar{\boldsymbol{A}}_{i,g} \in \mathbb{C}^{\mathring{N}_{\mathrm{BS}} \times \mathring{N}_{\mathrm{RF}}}$ is the gth block-matrix with constant modulus entries, i.e., $\left|[\bar{\boldsymbol{A}}_{i,g}]_{[r,c]}\right| = 1$, where $[\bar{\boldsymbol{A}}_{i,g}]_{[r,c]}$ is the (r,c)th entry of $\bar{\boldsymbol{A}}_{i,g}$.

Initially, we collect the measurement vectors $\{\bar{\boldsymbol{y}}_{k,i,j}\}_{j=1}^{T_{\mathrm{UE}}}$ next to each other as $\bar{\boldsymbol{Y}}_{k,i} = [\bar{\boldsymbol{y}}_{k,i,1}, \ldots, \bar{\boldsymbol{y}}_{k,i,T_{\mathrm{UE}}}]$, which can be written as

$$\bar{\boldsymbol{Y}}_{k,i} = \bar{\boldsymbol{A}}_i^{\mathsf{H}} \boldsymbol{H}_k \boldsymbol{F}_k + \bar{\boldsymbol{A}}_i^{\mathsf{H}} \bar{\boldsymbol{Z}}_{k,i} \in \mathbb{C}^{N_{\mathrm{RF}} \times T_{\mathrm{UE}}}, \tag{3}$$

where $\boldsymbol{F}_k = [\boldsymbol{f}_{k,1} s_{k,1}, \ldots, \boldsymbol{f}_{k,T_{\mathrm{UE}}} s_{k,T_{\mathrm{UE}}}] \in \mathbb{C}^{N_{\mathrm{UE}} \times T_{\mathrm{UE}}}$ and $\bar{\boldsymbol{Z}}_{k,i} = [\bar{\boldsymbol{z}}_{k,i,1}, \ldots, \bar{\boldsymbol{z}}_{k,i,T_{\mathrm{UE}}}]$. We assume that $\boldsymbol{F}_k, \forall k$, are designed with orthonormal rows, i.e., $\boldsymbol{F}_k \boldsymbol{F}_k^{\mathsf{H}} = \boldsymbol{I}_{N_{\mathrm{UE}}}, \forall k$, and $T_{\mathrm{UE}} \geq N_{\mathrm{UE}}$. After applying the right-filtering to (3) we obtain

$$\boldsymbol{Y}_{k,i} = \bar{\boldsymbol{Y}}_{k,i} \boldsymbol{F}^{\mathsf{H}} = \bar{\boldsymbol{A}}_i^{\mathsf{H}} \boldsymbol{H}_k + \boldsymbol{Z}_{k,i} \in \mathbb{C}^{N_{\mathrm{RF}} \times N_{\mathrm{UE}}}, \tag{4}$$

where $\boldsymbol{Z}_{k,i} = \bar{\boldsymbol{A}}_i^{\mathsf{H}} \bar{\boldsymbol{Z}}_{k,i} \boldsymbol{F}_k^{\mathsf{H}}$. Next, we collect the measurement matrices $\{\boldsymbol{Y}_{k,i}\}_{i=1}^{T_{\mathrm{BS}}}$ on the top of each other as $\boldsymbol{Y}_k = [\boldsymbol{Y}_{k,1}^{\mathsf{T}}, \ldots, \boldsymbol{Y}_{k,T_{\mathrm{BS}}}^{\mathsf{T}}]^{\mathsf{T}}$, which can be written as

$$\boldsymbol{Y}_k = \boldsymbol{A} \boldsymbol{H}_k + \boldsymbol{Z}_k \in \mathbb{C}^{L \times N_{\mathrm{UE}}}, \tag{5}$$

where $L = T_{\mathrm{BS}} N_{\mathrm{RF}}$, $\boldsymbol{A} = [\bar{\boldsymbol{A}}_1, \ldots, \bar{\boldsymbol{A}}_{T_{\mathrm{BS}}}]^{\mathsf{H}} \in \mathbb{C}^{L \times N_{\mathrm{BS}}}$, and $\boldsymbol{Z}_k = [\boldsymbol{Z}_{k,1}^{\mathsf{T}}, \ldots, \boldsymbol{Z}_{k,T_{\mathrm{BS}}}^{\mathsf{T}}]^{\mathsf{T}}$. After that, we collect the measurement matrices $\{\boldsymbol{Y}_k\}_{k=1}^{N_{\mathrm{SC}}}$ next to each other as $\boldsymbol{Y} = [\boldsymbol{Y}_1, \ldots, \boldsymbol{Y}_{N_{\mathrm{SC}}}]$, which can be written as

$$\boldsymbol{Y} = \boldsymbol{A} \boldsymbol{H} + \boldsymbol{Z} \in \mathbb{C}^{L \times N_{\mathrm{UE}} N_{\mathrm{SC}}}, \tag{6}$$

where $\boldsymbol{Z} = [\boldsymbol{Z}_1, \ldots, \boldsymbol{Z}_{N_{\mathrm{SC}}}]$ and $\boldsymbol{H} = [\boldsymbol{H}_1, \ldots, \boldsymbol{H}_{N_{\mathrm{SC}}}] \in \mathbb{C}^{N_{\mathrm{BS}} \times N_{\mathrm{UE}} N_{\mathrm{SC}}}$ is the total MIMO channel matrix.

Given the measurement matrix in (6), a LS-based method can be used to obtain an estimate of the total MIMO channel matrix as [14]

$$\hat{\boldsymbol{H}}_{\mathrm{LS}} = [\boldsymbol{A}]^{+} \boldsymbol{Y} = \left[\hat{\boldsymbol{H}}_1, \ldots, \hat{\boldsymbol{H}}_{N_{\mathrm{SC}}}\right] \in \mathbb{C}^{N_{\mathrm{BS}} \times N_{\mathrm{UE}} N_{\mathrm{SC}}}, \tag{7}$$

[1]To simplify the exposition, we assume that N_{BS}, N_{RF}, and N_{G} are selected so that $\mathring{N}_{\mathrm{BS}}$ and $\mathring{N}_{\mathrm{RF}}$ are integer numbers, without loss of generality.

[2]Note that if $N_{\mathrm{G}} = 1$, the above analog structure coincides with the known fully-connected analog structure [5], where every RF chain is connected to every antenna element. On the other hand, if $N_{\mathrm{G}} = N_{\mathrm{RF}}$, the above analog structure coincides with the known partially-connected analog structure [5], where every RF chain is connected to a unique subset of antenna elements.

where $[\boldsymbol{A}]^{+} = \boldsymbol{A}^{\mathrm{H}}(\boldsymbol{A}\boldsymbol{A}^{\mathrm{H}})^{-1}$ is the Moore-Penrose pseudo-inverse of $\boldsymbol{A}$. Note that, due to the left filtering, the LS-based method requires that $L \geq N_{\mathrm{BS}}$, i.e., $T_{\mathrm{BS}} \geq \frac{N_{\mathrm{BS}}}{N_{\mathrm{RF}}}$ to provide an accurate channel estimate. On the other hand, the LMMSE estimator of $\boldsymbol{H}$ can be written as [14]

$$\hat{\boldsymbol{H}}_{\mathrm{LMMSE}} = \boldsymbol{R}_{\boldsymbol{H}}\boldsymbol{A}^{\mathrm{H}}\left(\boldsymbol{A}\boldsymbol{R}_{\boldsymbol{H}}\boldsymbol{A}^{\mathrm{H}} + \sigma_n^2\boldsymbol{I}_L\right)^{-1}\boldsymbol{Y}, \tag{8}$$

where $\boldsymbol{R}_{\boldsymbol{H}} = \mathbb{E}\{\boldsymbol{H}\boldsymbol{H}^{\mathrm{H}}\}$ is the statistical channel correlation matrix of $\boldsymbol{H}$ [15], [16].

III. The Proposed SALSA Method

To obtain a more accurate channel estimate while reducing the training overhead, we propose in this section a novel channel estimation method called **SALSA**, which is derived by exploiting a hidden tensor structure in the measurement matrix in (6). To show this, we first recall the following propositions from [26], [27], [28].

Proposition 1: Let $\boldsymbol{X}$ be a matrix given as

$$\boldsymbol{X} = \boldsymbol{X}_1 \otimes \boldsymbol{X}_2 = \begin{bmatrix} \boldsymbol{X}_{1,1} & \dots & \boldsymbol{X}_{1,J_1} \\ \dots & & \\ \boldsymbol{X}_{I_1,1} & \dots & \boldsymbol{X}_{I_1,J_1} \end{bmatrix} \in \mathbb{C}^{I\times J}, \tag{9}$$

where $\boldsymbol{X}_1 \in \mathbb{C}^{I_1\times J_1}$, $\boldsymbol{X}_2 \in \mathbb{C}^{I_2\times J_2}$, $I = I_1I_2$, $J = J_1J_2$, and $\boldsymbol{X}_{n,m} = [\boldsymbol{X}_1]_{[n,m]}\boldsymbol{X}_2$ is the (n,m)th block-matrix of $\boldsymbol{X}$. Let $\boldsymbol{K} \in \mathbb{C}^{I_1J_1\times I_2J_2}$ be a rank-one matrix given as

$$\begin{aligned}\boldsymbol{K} &= \mathrm{stack}\{\mathrm{vec}\{\boldsymbol{X}_{1,1}\}^{\mathrm{T}}, \dots, \mathrm{vec}\{\boldsymbol{X}_{I_1,1}\}^{\mathrm{T}}, \dots, \mathrm{vec}\{\boldsymbol{X}_{I_1,J_1}\}^{\mathrm{T}}\} \\ &= \mathrm{vec}\{\boldsymbol{X}_1\}\mathrm{vec}\{\boldsymbol{X}_2\}^{\mathrm{T}},\end{aligned} \tag{10}$$

with the rank-one truncated-SVD given as $\boldsymbol{K} = \sigma\boldsymbol{u}\boldsymbol{v}^{\mathrm{H}}$, where $\boldsymbol{u} \in \mathbb{C}^{I_1J_1}$ and $\boldsymbol{v} \in \mathbb{C}^{I_2J_2}$ are the left and right singular vectors of $\boldsymbol{K}$, respectively, and σ is the associated singular value. Then, the optimal solution to

$$\underset{\boldsymbol{X}_1,\boldsymbol{X}_2}{\text{minimize}} \; \|\boldsymbol{X} - (\boldsymbol{X}_1 \otimes \boldsymbol{X}_2)\|_{\mathrm{F}}^2 \tag{11}$$

can be obtained as

$$\boldsymbol{X}_1 = \mathrm{reshape}\{\sqrt{\sigma}\boldsymbol{u}, I_1, J_1\} \tag{12}$$

$$\boldsymbol{X}_2 = \mathrm{reshape}\{\sqrt{\sigma}\boldsymbol{v}^{*}, I_2, J_2\}. \tag{13}$$

Proof: Please refer to [27] for more details.

Proposition 2: For any given $I \times J$ matrix $\boldsymbol{X}$, it can be *approximately* written as a summation of $R \geq 1$ factor matrices as

$$\boldsymbol{X} = \sum_{r=1}^{R}\boldsymbol{X}_r = \sum_{r=1}^{R}\boldsymbol{X}_{1,r} \otimes \boldsymbol{X}_{2,r}, \tag{14}$$

where $\boldsymbol{X}_r = \boldsymbol{X}_{1,r} \otimes \boldsymbol{X}_{2,r}$, $\boldsymbol{X}_{1,r} \in \mathbb{C}^{I_1\times J_1}$, and $\boldsymbol{X}_{2,r} \in \mathbb{C}^{I_2\times J_2}$, $I = I_1I_2$, and $J = J_1J_2$.

Proof: The proof follows directly by applying Proposition 1 sequentially [28]. The corresponding Proposition is summarized in Algorithm 1.

Let $I = N_{\mathrm{BS}}$ and $J = N_{\mathrm{UE}}N_{\mathrm{SC}}$. Then, from Proposition 2, the total frequency-domain MIMO channel matrix $\boldsymbol{H} \in \mathbb{C}^{I\times J}$ in (6) can be *approximately* written as

$$\boldsymbol{H} \approx \sum_{r=1}^{R}\boldsymbol{C}_r \otimes \boldsymbol{B}_r \in \mathbb{C}^{I\times J}, \tag{15}$$

where $\boldsymbol{B}_r \in \mathbb{C}^{I_1\times J_1}$, $\boldsymbol{C}_r \in \mathbb{C}^{I_2\times J_2}$, $I = I_1I_2$, and $J = J_1J_2$. As shown in Fig. 2, the *approximation* becomes tighter as the number of channel factor matrices R increases. More importantly, we can see that in case of full rank channels, the optimal value of R, denoted in the figure by R_{opt}, is dependent on the division scenario of I and J, where $R_{\mathrm{opt}} \approx \min\{I_1J_1, I_2J_2\}$. In other words, reducing the dimension of one of the channel factor matrices, i.e., $\boldsymbol{B}_r \in \mathbb{C}^{I_1\times J_1}$ or $\boldsymbol{C}_r \in \mathbb{C}^{I_2\times J_2}$, reduces the value of R_{opt}.

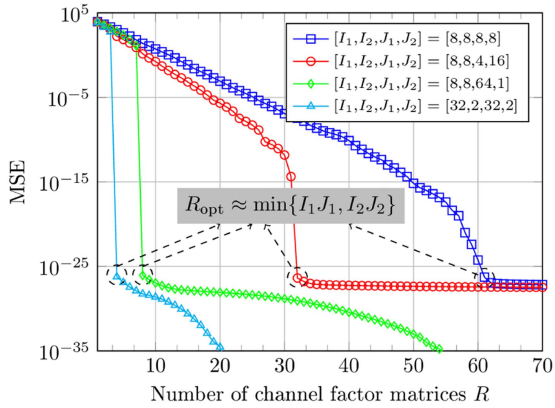

Fig. 2. MSE vs. the number of channel factor matrices R assuming $N_{\mathrm{BS}} = 64$, $N_{\mathrm{UE}} = 4$, and $N_{\mathrm{SC}} = 16$, where $\mathrm{MSE} = \|\boldsymbol{H} - \sum_{r=1}^{R}\boldsymbol{C}_r \otimes \boldsymbol{B}_r\|_{\mathrm{F}}^2$. Here, the total MIMO channel matrix $\boldsymbol{H} = [\boldsymbol{H}_1, \dots, \boldsymbol{H}_{N_{\mathrm{SC}}}] \in \mathbb{C}^{I\times J}$ is generated following the 3GPP CDL channel model [24], [25] with the main system parameters outlined in Table I in Section IV.

Algorithm 1: Sequential Kronecker Factorization.

1: **Input**: A matrix $\boldsymbol{X} \in \mathbb{C}^{I\times J}$
2: Select R, I_1, J_1, I_2, J_2 such that $I = I_1I_2$ and $J = J_1J_2$
3: **for** $r = 1$ to R **do**
4: Get $\boldsymbol{X}_r = \boldsymbol{X} - \sum_{r'=1}^{r-1}\boldsymbol{X}_{1,r'} \otimes \boldsymbol{X}_{2,r'}$
5: Given $\boldsymbol{X}_r$, get $\boldsymbol{X}_{1,r}$ and $\boldsymbol{X}_{2,r}$ using (12) and (13), respectively
6: **end for**
7: **Output**: $\hat{\boldsymbol{X}} = \sum_{r=1}^{R}\boldsymbol{X}_{1,r} \otimes \boldsymbol{X}_{2,r} \in \mathbb{C}^{I\times J}$

Let $L = T_{\mathrm{BS}}N_{\mathrm{RF}}$. Then, by substituting (15) into (6), and assuming R is sufficiently large, e.g., $R \geq \min\{I_1J_1, I_2J_2\}$, we can write

$$\begin{aligned}\boldsymbol{Y} &= \boldsymbol{A}\left(\sum_{r=1}^{R}\boldsymbol{C}_r \otimes \boldsymbol{B}_r\right) + \boldsymbol{Z} = \sum_{r=1}^{R}\boldsymbol{A}(\boldsymbol{C}_r \otimes \boldsymbol{B}_r) + \boldsymbol{Z} \\ &= \sum_{r=1}^{R}\boldsymbol{Y}_r + \boldsymbol{Z} \in \mathbb{C}^{L\times J},\end{aligned} \tag{16}$$

where $\boldsymbol{Y}_r = \boldsymbol{A}(\boldsymbol{C}_r \otimes \boldsymbol{B}_r) \in \mathbb{C}^{L\times J}$. Note that $\boldsymbol{Y}_r$ can be seen as the 1-mode unfolding of a 3-way Tucker tensor given as

$$\boldsymbol{\mathcal{Y}}_r = \boldsymbol{\mathcal{S}} \times_1 \boldsymbol{A} \times_2 \boldsymbol{B}_r^{\mathrm{T}} \times_3 \boldsymbol{C}_r^{\mathrm{T}} \in \mathbb{C}^{L\times J_1\times J_2}, \tag{17}$$

where $\boldsymbol{\mathcal{S}} \in \mathbb{Z}^{I\times I_1\times I_2}$ is the core-tensor with the 1-mode unfolding given as $[\boldsymbol{\mathcal{S}}]_{(1)} \overset{\mathrm{def}}{=} \boldsymbol{I}_I$ [17]. The ℓ-mode unfolding of $\boldsymbol{\mathcal{Y}}_r$, $\ell = \{1,2,3\}$, can be expressed as

$$[\boldsymbol{\mathcal{Y}}_r]_{(1)} = \boldsymbol{A}[\boldsymbol{\mathcal{S}}]_{(1)}(\boldsymbol{C}_r \otimes \boldsymbol{B}_r) \in \mathbb{C}^{L\times J}, \tag{18}$$

$$[\boldsymbol{\mathcal{Y}}_r]_{(2)} = \boldsymbol{B}_r^{\mathrm{T}}[\boldsymbol{\mathcal{S}}]_{(2)}(\boldsymbol{C}_r \otimes \boldsymbol{A}^{\mathrm{T}}) \in \mathbb{C}^{J_1\times LJ_2}, \tag{19}$$

$$[\boldsymbol{\mathcal{Y}}_r]_{(3)} = \boldsymbol{C}_r^{\mathrm{T}}[\boldsymbol{\mathcal{S}}]_{(3)}(\boldsymbol{B}_r \otimes \boldsymbol{A}^{\mathrm{T}}) \in \mathbb{C}^{J_2\times LJ_1}. \tag{20}$$

Algorithm 2: SALSA For MIMO-OFDM Channel Estimation.

Input: Measurement matrix $\boldsymbol{Y} \in \mathbb{C}^{L\times J}$ as in (6)
Select $R \geq 1$, $N_{\text{max-iter}} \geq 1$, I_1, I_2, J_1, and J_2 such that $I = I_1 I_2 = N_{\text{BS}}$ and $J = J_1 J_2 = N_{\text{UE}} N_{\text{SC}}$
Obtain the 3-way Tucker tensor $\boldsymbol{\mathcal{Y}}$ in (21) from $\boldsymbol{Y}$
for $r = 1$ to R **do**
  Get $\boldsymbol{\mathcal{Y}}_r = \boldsymbol{\mathcal{Y}} - \sum_{r'=1}^{r-1} \hat{\boldsymbol{\mathcal{Y}}}_{r'}$
  Initialize $\boldsymbol{C}_r^{(0)} \in \mathbb{C}^{I_2\times J_2}$, e.g., randomly
  for $n = 1$ to $N_{\text{max-iter}}$ **do**
    Get $\boldsymbol{B}_r^{(n)}$ using (23) for given $\boldsymbol{C}_r^{(n-1)}$
    Get $\boldsymbol{C}_r^{(n)}$ using (24) for given $\boldsymbol{B}_r^{(n)}$
  end for
  Set $\hat{\boldsymbol{B}}_r = \boldsymbol{B}_r^{(N_{\text{max-iter}})}$ and $\hat{\boldsymbol{C}}_r = \boldsymbol{C}_r^{(N_{\text{max-iter}})}$
  Get $\hat{\boldsymbol{\mathcal{Y}}}_r = \boldsymbol{\mathcal{S}} \times_1 \boldsymbol{A} \times_2 \hat{\boldsymbol{B}}_r^{\mathsf{T}} \times_3 \hat{\boldsymbol{C}}_r^{\mathsf{T}}$, go back to Step (5)
end for
Output: $\hat{\boldsymbol{H}}_{\text{SALSA}} = \sum_{r=1}^{R} \hat{\boldsymbol{C}}_r \otimes \hat{\boldsymbol{B}}_r \in \mathbb{C}^{I\times J}$

From (17), the 3-way Tucker tensor form of (16) can be expressed as

$$\boldsymbol{\mathcal{Y}} = \sum_{r=1}^{R} \boldsymbol{\mathcal{Y}}_r + \boldsymbol{\mathcal{Z}} \in \mathbb{C}^{L\times J_1\times J_2}, \tag{21}$$

where $\boldsymbol{\mathcal{Z}}$ is the 3-way tensor representation of the noise matrix $\boldsymbol{Z}$. This latter formulation suggests that the factor matrices $\{\boldsymbol{B}_r, \boldsymbol{C}_r\}_{r=1}^{R}$ can be estimated sequentially as follows. Let $\boldsymbol{\mathcal{Y}}_r$ be the tensor obtained at the rth sequential step as

$$\boldsymbol{\mathcal{Y}}_r = \boldsymbol{\mathcal{Y}} - \sum_{r'=1}^{r-1} \boldsymbol{\mathcal{Y}}_{r'} \in \mathbb{C}^{L\times J_1\times J_2}. \tag{22}$$

Then, by exploiting the 2-mode and the 3-mode unfoldings, the rth factor matrices $\boldsymbol{B}_r$ and $\boldsymbol{C}_r$ can be obtained using, e.g., the ALS method [18], where one factor matrix is assumed to be fixed when solving for the other. Specifically, $\boldsymbol{B}_r$ and $\boldsymbol{C}_r$ can be obtained as

$$\boldsymbol{B}_r^{\mathsf{T}} = [\boldsymbol{\mathcal{Y}}_r]_{(2)} [\boldsymbol{\Psi}_2]^{+} = [\boldsymbol{\mathcal{Y}}_r]_{(2)} \boldsymbol{\Psi}_2^{\mathsf{H}} [\boldsymbol{\Psi}_2 \boldsymbol{\Psi}_2^{\mathsf{H}}]^{-1} \tag{23}$$

$$\boldsymbol{C}_r^{\mathsf{T}} = [\boldsymbol{\mathcal{Y}}_r]_{(3)} [\boldsymbol{\Psi}_3]^{+} = [\boldsymbol{\mathcal{Y}}_r]_{(3)} \boldsymbol{\Psi}_3^{\mathsf{H}} [\boldsymbol{\Psi}_3 \boldsymbol{\Psi}_3^{\mathsf{H}}]^{-1}, \tag{24}$$

where $\boldsymbol{\Psi}_2$ and $\boldsymbol{\Psi}_3$ are given as

$$\boldsymbol{\Psi}_2 = [\boldsymbol{\mathcal{S}}]_{(2)} (\boldsymbol{C}_r \otimes \boldsymbol{A}^{\mathsf{T}}) \in \mathbb{C}^{I_1\times LJ_2} \tag{25}$$

$$\boldsymbol{\Psi}_3 = [\boldsymbol{\mathcal{S}}]_{(3)} (\boldsymbol{B}_r \otimes \boldsymbol{A}^{\mathsf{T}}) \in \mathbb{C}^{I_2\times LJ_1}. \tag{26}$$

Algorithm 2 summarizes the proposed SALSA method for estimating the total MIMO channel matrix $\boldsymbol{H} \in \mathbb{C}^{I\times J}$, which is guaranteed to converge monotonically to, at least, a local optimum solution [18].

Note that, due to the right filtering, the SALSA method in Algorithm 2 requires that (C1) $I_1 \leq LJ_2$ and (C2) $I_2 \leq LJ_1$, i.e., $T_{\text{BS}} \geq \min\{\frac{I_1}{N_{\text{RF}} J_2}, \frac{I_2}{N_{\text{RF}} J_1}\}$ to provide an accurate channel estimation. Therefore, under practical settings, the SALSA method in Algorithm 2 requires less training overhead than the LS method in (7). On the other hand, assuming that the complexity of calculating the Moore-Penrose pseudo-inverse of an $n \times m$ matrix is on the order of $\mathcal{O}(\min\{n, m\}^3)$, where $\mathcal{O}$ denotes the Big O notation, then the complexity of the LS method in (7) is on the order of $\mathcal{O}(\min\{L, J\})^3$, while for the SALSA method in Algorithm 2 the complexity is on the order of $\mathcal{O}(R \cdot N_{\text{max-iter}} \cdot I_1^3 \cdot I_2^3)$, assuming that the (C1) and (C2) conditions are satisfied. Moreover, for LMMSE in (8), the complexity is on the order of $\mathcal{O}(L^3)$, assuming that the complexity of calculating the inverse of an $n \times n$ matrix is on the order of $\mathcal{O}(n^3)$.

TABLE I
SYSTEM PARAMETERS

Parameter	Value
Scenario	UMi
Cell radius	100 m
BS (UE) height	10 (1.5) m
Carrier frequency f_c	4 GHz
Sampling frequency f_s	30.72 MSamples/s
No. of subcarriers N_{SC}	16
No. of antennas at BS N_{BS}	16 (4×4) or 64 (8×8)
No. of antennas at UE N_{UE}	4 (2×2)
Polarization	Single

IV. SIMULATION RESULTS

We adopt the 3GPP CDL channel model described in TR 38.901 [24], where a step-by-step tutorial of it along the MATLAB scripts for channel generation is presented in [25]. Specifically, in our simulation, we first generate a time-domain channel tensor $\boldsymbol{\mathcal{H}} \in \mathbb{C}^{N_{\text{BS}}\times N_{\text{UE}}\times N_{\text{taps}}}$, where N_{taps} represents the number of time-domain channel taps calculated according to [25, Eqn. (64)] and using the system parameters shown in Table I. Then, we perform a N_{SC}-point FFT operation along the third dimension for each receive-transmit antenna pair to obtain the frequency-domain channel tensor $\boldsymbol{\mathcal{H}} \in \mathbb{C}^{N_{\text{BS}}\times N_{\text{UE}}\times N_{\text{SC}}}$, where the kth slice matrix, i.e., $\boldsymbol{H}_k = \boldsymbol{\mathcal{H}}_{[:,:,k]} \in \mathbb{C}^{N_{\text{BS}}\times N_{\text{UE}}}$ represents the kth subcarrier frequency-domain MIMO channel matrix.

We show the simulation results in terms of the normalized mean-square-error (NMSE) that is defined as $\text{NMSE} = \mathbb{E}\{\|\boldsymbol{H} - \hat{\boldsymbol{H}}_{\text{X}}\|_{\text{F}}^2\}/\mathbb{E}\|\boldsymbol{H}\|_{\text{F}}^2\}$, where $\text{X} \in \{\text{LS, LMMSE, SALSA}\}$. The signal-to-noise ratio (SNR) is defined as $\text{SNR} = \mathbb{E}\{\|\boldsymbol{\mathcal{Y}} - \boldsymbol{\mathcal{Z}}\|_{\text{F}}^2\}/\mathbb{E}\{\|\boldsymbol{\mathcal{Z}}\|_{\text{F}}^2\}$. In all simulation scenarios, we set $N_{\text{UE}} = 4$, $N_{\text{SC}} = 16$, $T_{\text{UE}} = N_{\text{UE}} = 4$, $N_{\text{RF}} = 4$, $N_{\text{G}} = 2$, and assume a random generation of the analog decoding matrix $\boldsymbol{A} \in \mathbb{C}^{T_{\text{BS}} N_{\text{RF}}\times N_{\text{BS}}}$, where every nonzero entry is obtained as $a = 1/\sqrt{N_{\text{BS}}} \cdot e^{j\phi}$, where $\phi \in [0, 2\pi]$.

For the LMMSE method, we assume that the statistical channel correlation matrix, i.e., $\boldsymbol{R}_{\boldsymbol{H}}$, is obtained as

$$\boldsymbol{R}_{\boldsymbol{H}} = \boldsymbol{R}_{\boldsymbol{H}}^{\text{true}} + \beta \cdot \boldsymbol{R}_{\boldsymbol{H}}^{\text{noise}}, \tag{27}$$

where $\boldsymbol{R}_{\boldsymbol{H}}^{\text{true}}$ is the true statistical channel correlation matrix obtained as an average of $T = 1000$ channel realizations, i.e.,

$$\boldsymbol{R}_{\boldsymbol{H}}^{\text{true}} = \frac{1}{T} \sum_{t=1}^{T} \boldsymbol{H}_t \boldsymbol{H}_t^{\mathsf{H}}, \tag{28}$$

with $\boldsymbol{H}_t = [\boldsymbol{H}_{t,1}, \ldots, \boldsymbol{H}_{t,N_{\text{SC}}}] \in \mathbb{C}^{N_{\text{BS}}\times N_{\text{UE}} N_{\text{SC}}}$ being the tth channel realization. Moreover, $\boldsymbol{R}_{\boldsymbol{H}}^{\text{noise}}$ is an additive-noise covariance matrix and β is a noise power scaling parameter obtained such that $\beta = \|\boldsymbol{R}_{\boldsymbol{H}} - \boldsymbol{R}_{\boldsymbol{H}}^{\text{true}}\|_{\text{F}}^2 / \|\boldsymbol{R}_{\boldsymbol{H}}^{\text{true}}\|_{\text{F}}^2$. Note that, $\beta = 0$ can be considered as the ideal scenario, which is used in [15] as a baseline approach for some $\boldsymbol{R}_{\boldsymbol{H}}$ estimation methods. On the other hand, for scenarios with $\beta > 0$, we demonstrate the impact of the estimation accuracy of $\boldsymbol{R}_{\boldsymbol{H}}$ on the estimation accuracy of the LMMSE method.

Initially, we assume that $N_{\text{BS}} = 64$ and show simulation results investigating the best division scenario of I and J with the constraints of $I = I_1 I_2$, $J = J_1 J_2$, $I_d \geq 1$, $J_d \geq 1$, and I_d, J_d are Natural numbers, where $d \in \{1, 2\}$. Recall that $I = N_{\text{BS}}$ and $J = N_{\text{UE}} N_{\text{SC}}$. Therefore, we have $I = J = 64$ and the candidate numbers of I_d and J_d are $1, 2, 4, 8, 16, 32$, and 64. Therefore, we have in total 49 different division scenarios, e.g., Scenario 1: $\{[I_1, I_2, J_1, J_2] = [64, 1, 64, 1]\}$ and Scenario 2: $\{[I_1, I_2, J_1, J_2] = [64, 1, 32, 2]\}$. We have simulated the

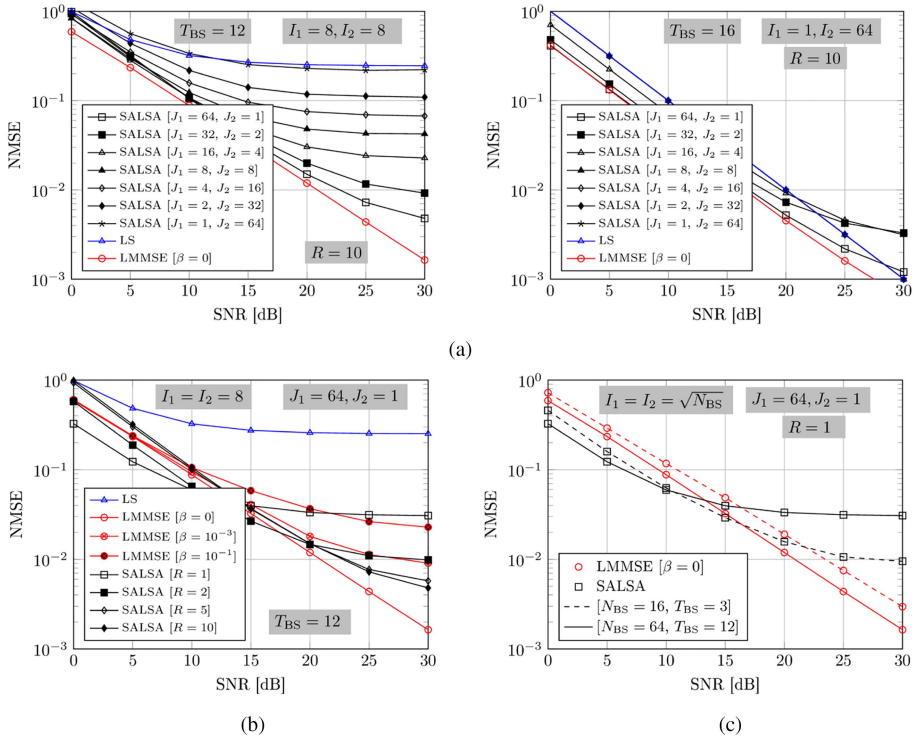

Fig. 3. NMSE vs. SNR for different simulation scenarios.

SALSA algorithm using all the 49 possible scenarios. In Fig. 3(a), we show the NMSE versus SNR results for some selected I and J division scenarios. The other scenarios are not shown, due to space limitations, but we note that their NMSE performance are inferior compared to the shown scenarios.

From Fig. 3(a), when $T_{\text{BS}} = 12$, i.e., $L = T_{\text{BS}} N_{\text{RF}} = 48 < N_{\text{BS}}$, the analog training matrix $\boldsymbol{A} \in \mathbb{C}^{L \times N_{\text{BS}}}$, i.e., the first factor matrix of the measurement tensor in (17), is left non-invertible, i.e., $[\boldsymbol{A}]^{+}\boldsymbol{A} \neq \boldsymbol{I}$. Therefore, the LS-based method has a very bad channel estimation accuracy. Differently, we can see that the LMMSE method provides the highest channel estimation accuracy, thanks to the prior knowledge of the statistical channel correlation matrix $\boldsymbol{R_H}$ and noise variance σ_n^2. On the other hand, we can see that the best NMSE of SALSA method is achieved when $I_1 = 8$, $I_2 = 8$, $J_1 = 64$, and $J_2 = 1$, i.e., when $\boldsymbol{B}_r \in \mathbb{C}^{8 \times 64}$ and $\boldsymbol{C}_r \in \mathbb{C}^{8 \times 1}, \forall r$. The main reason is that by dividing $I = 64$ equally between I_1 and I_2, i.e., $I_1 = I_2 = 8$, SALSA reduces the impact of the non-invertibility of $\boldsymbol{A}$ by distributing it between the second (i.e., $\boldsymbol{B}_r$) and the third (i.e., $\boldsymbol{C}_r$) factor matrices of the measurement tensor, which leads to a better channel estimation accuracy. On the other hand, by setting $J_1 = 64$ and $J_2 = 1$, the required number of channel factor matrices R reduces as compared to the other division scenario, as we have illustrated in Fig. 2.

Differently, when $T_{\text{BS}} = 16$, i.e., $L = N_{\text{BS}}$, the analog training matrix $\boldsymbol{A}$ is left invertible, i.e., $[\boldsymbol{A}]^{+}\boldsymbol{A} = \boldsymbol{I}$. Therefore, the LS-based method has a high channel estimation accuracy. Moreover, we can see that the LMMSE-based method maintains its superiority, providing the best channel estimation accuracy. For SALSA, we have noticed that the best channel estimation accuracy is obtained with the scenario of $[I_1, I_2, J_1, J_2] = [1, 64, 64, 1]$, i.e., when $\boldsymbol{B}_r \in \mathbb{C}^{1 \times 64}$ and $\boldsymbol{C}_r \in \mathbb{C}^{64 \times 1}$ (or, *not shown in the figure*, with scenario of $[I_1, I_2, J_1, J_2] = [64, 1, 1, 64]$, i.e., when $\boldsymbol{B}_r \in \mathbb{C}^{64 \times 1}$ and $\boldsymbol{C}_r \in \mathbb{C}^{1 \times 64}$). With both of these scenarios, the channel matrix $\boldsymbol{H} \in \mathbb{C}^{64 \times 64}$ in (15) is decomposed into a summation of R factor matrices $\boldsymbol{B}_r \otimes \boldsymbol{C}_r \in \mathbb{C}^{64 \times 64}$, each having a rank-one, i.e., $rank\{\boldsymbol{B}_r \otimes \boldsymbol{C}_r\} = 1, \forall r$, leading to a better estimation accuracy and approaching the LMMSE-based method.

In Fig. 3(b), we show the NMSE versus SNR results obtained by varying the number of channel factor matrices, i.e., R, and the noise-power scaling parameter of $\boldsymbol{R_H}$, i.e., β. Clearly, Fig. 3(b) shows that the channel estimation accuracy of LMMSE decreases as β increases, since increasing β imitates a decrease of the estimation accuracy of $\boldsymbol{R_H}$. On the other hand, Fig. 3(b) shows that the channel estimation accuracy of SALSA increases with the increasing R in the high SNR region (i.e., SNR $\geq$ 15 dB) while it decreases with the increasing R in the low SNR region (i.e., SNR $<$ 15 dB). The main reason is that, in the high SNR region, where the impact of noise is minimal, by increasing R we succesively estimate more factor matrices belonging to the subspace of the true channel matrix. This leads to a better channel estimation accuracy, as we have illustrated in Fig. 2 for noiseless channel matrices. On the other hand, the channel measurement tensor is noise limited in the low SNR region. Therefore, the sequentially estimated channel factor matrices become very noisy above a certain R as they mainly belong to the noise subspace. In other words, in this case, as R increases, the influence of the noise increases and the overall estimation accuracy decreases. Clearly, for every SNR level, there is an optimal R value (i.e., R_{opt}) wherein the channel estimation accuracy is maximized. We conjecture that R_{opt} is in function of the noise variance σ_n^2, which we leave for a follow up work.

Finally, in Fig. 3(c), we show NMSE versus SNR simulation results by varying the number of antenna elements at the BS, i.e., N_{BS}. For a fair comparison, we adjust the number of training blocks T_{BS} so that both considered scenarios have the same ratio of $\frac{L}{N_{\text{BS}}} = 0.75$ (recall that $L = T_{\text{BS}} N_{\text{RF}}$). From Fig. 3(c), we can observe that the SALSA method has a similar behavior for both N_{BS} scenarios. In the low SNR region, the SALSA method has a better channel estimation accuracy than LMMSE, while LMMSE has a better channel estimation accuracy than SALSA in the high SNR region. However, the main difference

is that with the smaller N_{BS} value (i.e., $N_{\text{BS}} = 16$ in the figure), the SALSA method, with fixed R value, maintains its estimation accuracy superiority over the LMMSE for a higher SNR level as compared to the scenario with the larger N_{BS} value (i.e., $N_{\text{BS}} = 64$ in the figure). This can be explained with reference to Fig. 2, which shows that the optimal R value (i.e., R_{opt}) is smaller with the smaller factor matrices (i.e., when $N_{\text{BS}} = 16$, we have $[I_1, I_2] = [4, 4]$ and, therefore, $R_{\text{opt}} \approx 4$, while when $N_{\text{BS}} = 64$, we have $[I_1, I_2] = [8, 8]$ and, therefore, $R_{\text{opt}} \approx 8$. Note that $[J_1, J_2] = [64, 1]$ for both scenarios).

V. Conclusion

In this article, we have proposed a novel channel estimation method for MIMO-OFDM sub-6 GHz communication systems called SALSA. We have shown that an accurate channel estimation can be obtained with a small training overhead by exploiting a hidden tensor structure in the received measurement matrix, which estimates the channel matrix sequentially using an ALS-based method. Our results show that the SALSA method outperforms the conventional LS-based method, especially in the low training overhead. Moreover, it is shown that SALSA, under some settings, outperforms LMMSE-based methods with an ideal knowledge of the statistical channel correlation matrix, in the low SNR region, while it approaches it in the high SNR region. Given that SALSA does not require the prior knowledge of the statistical channel correlation matrix, as compared to LMMSE, makes it more appealing for practical implementations.

References

[1] T. L. Marzetta, E. G. Larsson, H. Yang, and H. Q. Ngo, *Fundamentals of Massive MIMO.*, Cambridge, U.K.: Cambridge Univ. Press, 2016.

[2] E. Dahlman, S. Parkvall, and J. Skold, *5G NR: The Next Generation Wireless Access Technology*, 1st ed. Cambridge, MA, USA: Academic Press, 2018.

[3] E. Björnson, L. Sanguinetti, J. Hoydis, and M. Debbah, "Optimal design of energy-efficient multi-user MIMO systems: Is massive MIMO the answer?," *IEEE Trans. Wireless Commun.*, vol. 14, no. 6, pp. 3059–3075, Jun. 2015.

[4] R. W. Heath, N. González-Prelcic, S. Rangan, W. Roh, and A. M. Sayeed, "An overview of signal processing techniques for millimeter wave MIMO systems," *IEEE J. Sel. Topics Signal Process.*, vol. 10, no. 3, pp. 436–453, Apr. 2016.

[5] K. Ardah, G. Fodor, Y. C. B. Silva, W. C. Freitas, and F. R. P. Cavalcanti, "A unifying design of hybrid beamforming architectures employing phase-shifters or switches," *IEEE Trans. Veh. Technol.*, vol. 67, no. 11, pp. 11243–11247, Nov. 2018.

[6] X. Gao, L. Dai, S. Han, C.-L. I, and R. W. Heath, "Energy-efficient hybrid analog and digital precoding for MmWave MIMO systems with large antenna arrays," *IEEE J. Sel. Areas Commun.*, vol. 34, no. 4, pp. 998–1009, Apr. 2016.

[7] H. Shokri-Ghadikolaei, C. Fischione, G. Fodor, P. Popovski, and M. Zorzi, "Millimeter wave cellular networks: A MAC layer perspective," *IEEE Trans. Commun.*, vol. 63, no. 10, pp. 3437–3458, Oct. 2015.

[8] S. Gherekhloo, K. Ardah, and M. Haardt, "Hybrid beamforming design for downlink MU-MIMO-OFDM millimeter-wave systems," in *Proc. IEEE 11th Sensor Array Multichannel Signal Process. Workshop*, 2020, pp. 1–5.

[9] A. Alkhateeb, G. Leus, and R. W. Heath, "Compressed sensing based multi-user millimeter wave systems: How many measurements are needed?," in *Proc. IEEE Int. Conf. Acoust., Speech Signal Process.*, 2015, pp. 2909–2913.

[10] K. Ardah, B. Sokal, A. L. F. de Almeida, and M. Haardt, "Compressed sensing based channel estimation and open-loop training design for hybrid analog-digital massive MIMO systems," in *Proc. IEEE Int. Conf. Acoust., Speech Signal Process.*, 2020, pp. 4597–4601.

[11] J. Zhang and M. Haardt, "Channel estimation and training design for hybrid multi-carrier mmwave massive MIMO systems: The beamspace ESPRIT approach," in *Proc. IEEE 25th Eur. Signal Process. Conf.*, 2017, pp. 385–389.

[12] X. Hu, C. Liu, M. Peng, and C. Zhong, "IRS-based integrated location sensing and communication for mmwave SIMO systems," *IEEE Trans. Wireless Commun.*, vol. 22, no. 6, pp. 4132–4145, Jun. 2023.

[13] I. Barhumi, G. Leus, and M. Moonen, "Optimal training design for MIMO OFDM systems in mobile wireless channels," *IEEE Trans. Signal Process.*, vol. 51, no. 6, pp. 1615–1624, Jun. 2003.

[14] M. Biguesh and A. B. Gershman, "Training-based MIMO channel estimation: A study of estimator tradeoffs and optimal training signals," *IEEE Trans. Signal Process.*, vol. 54, no. 3, pp. 884–893, Mar. 2006.

[15] F. A. Dietrich, T. Ivanov, and W. Utschick, "Estimation of channel and noise correlations for MIMO channel estimation," in *Proc. Int. ITG Workshop Smart Antennas*, 2006, pp. 1–7.

[16] K. Upadhya and S. A. Vorobyov, "Covariance matrix estimation for massive MIMO," *IEEE Signal Process. Lett.*, vol. 25, no. 4, pp. 546–550, Apr. 2018.

[17] M. Haardt, F. Roemer, and G. Del Galdo, "Higher-order SVD-based subspace estimation to improve the parameter estimation accuracy in multidimensional harmonic retrieval problems," *IEEE Trans. Signal Process.*, vol. 56, no. 7, pp. 3198–3213, Jul. 2008.

[18] P. Comon, X. Luciani, and A. L. F. de Almeida, "Tensor decompositions, alternating least squares and other tales," *J. Chemometrics*, vol. 23, no. 7-8, pp. 393–405, 2009.

[19] A. L. F. de Almeida, "Tensor modeling and signal processing for wireless communication systems," Theses, Université de Nice Sophia Antipolis, Sophia Antipolis, France, Nov. 2007. [Online]. Available: https://theses.hal.science/tel-00460157

[20] M. N. da Costa, G. Favier, and J. M. T. Romano, "Tensor modelling of MIMO communication systems with performance analysis and kronecker receivers," *Signal Process.*, vol. 145, pp. 304–316, 2018.

[21] Z. Lin, T. Lv, W. Ni, J. A. Zhang, and R. P. Liu, "Tensor-based multidimensional wideband channel estimation for mmWave hybrid cylindrical arrays," *IEEE Trans. Commun.*, vol. 68, no. 12, pp. 7608–7622, Dec. 2020.

[22] C. Qian, X. Fu, N. D. Sidiropoulos, and Y. Yang, "Tensor-based channel estimation for dual-polarized massive MIMO systems," *IEEE Trans. Signal Process.*, vol. 66, no. 24, pp. 6390–6403, Dec. 2018.

[23] S. Gherekhloo, K. Ardah, A. L. de Almeida, and M. Haardt, "Tensor-based channel estimation and reflection design for RIS-aided millimeter-wave MIMO communication systems," in *Proc. IEEE 55th Asilomar Conf. Signals, Syst., Comput.*, 2021, pp. 1683–1689.

[24] 3rd Generation Partnership Project (3GPP), "Study on Channel Model for Frequencies from 0.5 to 100 GHz," 3GPP, Sophia Antipolis, France, Tech. Rep. 38.901 V16.1.0, 2020.

[25] D. G. Riviello, F. Di Stasio, and R. Tuninato, "Performance analysis of multi-user MIMO schemes under realistic 3GPP 3-D channel model for 5G mmwave cellular networks," *Electronics*, vol. 11, no. 3, 2022, Art. no. 330. [Online]. Available: https://www.mdpi.com/2079-9292/11/3/330

[26] C. F. Van Loan and N. Pitsianis, *Approximation With Kronecker Products*, M. S. Moonen, G. H. Golub, and B. L. R. De Moor, Eds. Dordrecht, The Netherlands:Springer, 1993.

[27] K. K. Wu, Y. Yam, H. Meng, and M. Mesbahi, "Kronecker product approximation with multiple factor matrices via the tensor product algorithm," in *Proc. IEEE Int. Conf. Syst., Man, Cybern.*, 2016, pp. 004277–004282.

[28] C. Garvey, C. Meng, and J. G. Nagy, "Singular value decomposition approximation via kronecker summations for imaging applications," *SIAM J. Matrix Anal. Appl.*, vol. 39, no. 4, pp. 1836–1857, 2018.